IEEE Access
Multidisciplinary | Rapid Review | Open Access Journal

Received October 31, 2018, accepted November 8, 2018, date of publication November 12, 2018,
date of current version December 18, 2018.

Digital Object Identifier 10.1109/ACCESS.2018.2880905

Relationship of External Field Strength With Local and Whole-Body Averaged Specific Absorption Rates in Anatomical Human Models

KENJI TAGUCHI[1], ILKKA LAAKSO[2], (Member, IEEE), KATSUAKI AGA[3], AKIMASA HIRATA[3], (Fellow, IEEE), YINLIANG DIAO[4], (Member, IEEE), JERDVISANOP CHAKAROTHAI[5], (Member, IEEE), AND TATSUYA KASHIWA[1], (Member, IEEE)

[1]Kitami Institute of Technology, Kitami 090-8507, Japan
[2]Department of Electrical Engineering and Automation, Aalto University, 02150 Espoo, Finland
[3]Department of Electrical and Mechanical Engineering, Nagoya Institute of Technology, Nagoya 466-8555, Japan
[4]South China Agricultural University, Guangzhou 510642, China
[5]National Institute of Information and Communications Technology, Tokyo 184-8795, Japan

Corresponding authors: Kenji Taguchi (ktaguchi@mail.kitami-it.ac.jp) and Akimasa Hirata (ahirata@nitech.ac.jp)

This work was supported by JSPS KAKENHI under Grant JP17K06288 and Grant JP18K04077.

ABSTRACT The International Commission on Non-Ionizing Radiation Protection (ICNIRP) guidelines and the IEEE C95.1 standard are currently under revision. In the guidelines/standard, the dominant effect for electromagnetic field exposures at frequencies above 100 kHz is the thermal effect. The whole-body- and 10g-averaged specific absorption rates (SARs), which are surrogates for core and local temperature elevations, respectively, are set as metrics for exposure evaluation. The external field strengths or incident power density, corresponding to the limit for SARs, are also used as metrics for practical compliance purposes. Although the limits for the SARs are identical amongst the guidelines/standard, the limits for the external field strengths differ by a factor of 7.4–12.9 in an intermediate frequency range (100 kHz–100 MHz). Due to the fact that the standard/guidelines were published before the computation with anatomical human models was available, it is worth revisiting the relationship between the SARs and external field strengths by computations using the human models. Intercomparison using different numerical codes was also performed to verify the results. For the main finding, as expected, the 10g-averaged SAR was a less restrictive factor for whole-body exposure over the frequencies considered in this paper. It was also found that the relationship between SARs and external field strength was satisfied, but was more conservative in the ICNIRP guidelines, whereas there were slight discrepancies below 30 MHz in the IEEE standard. The computational results would be useful for revising the permissible external field strength based on scientific results.

INDEX TERMS Dosimetry, biological effects of radiation, standardization, radiation safety.

I. INTRODUCTION

The World Health Organization (WHO) reviews scientific literature on potential adverse health effects caused by electromagnetic field exposures, and its conclusion is summarized as the Environmental Health Criteria Monograph. A monograph is now being prepared for radio-frequency field. Based on the review, international standardization bodies provide a recommendation for human safety from electromagnetic fields. For frequencies lower than 300 GHz, the International Commission on Non-Ionizing Radiation Protection (ICNIRP) guidelines [1] and the IEEE International Committee on Electromagnetic Safety standard [2], [3] are referred to in the WHO documents. The guidelines and standard from these two international organizations are currently under revision for frequency ranges between 100 kHz and 300 GHz in [1] and from 0 Hz to 300 GHz in [2] and [3]. In the frequency range above 100 kHz, the thermal effect is dominant.

In the guidelines/standard [1], [3], the specific absorption rate (SAR), which is defined as the power absorption per unit mass, is used as the internal physical quantity. The whole-body averaged SAR is used for whole-body exposure, while the peak value of SAR averaged over 10 g of tissue is used for

localized exposure. These metrics are introduced to prevent excess core and local temperature elevations, respectively. The limit for internal physical quantities is referred to as 'basic restriction' (BR) and 'dosimetric exposure limit' in the ICNIRP guidelines and in the IEEE standard, respectively. Since the dosimetric exposure limit was referred to as BR until the revision of C95.1 in 2005 [3], we thus refer to the limit for the internal physical quantities as the BR henceforth.

It is difficult or virtually impossible to measure the SAR or the internal physical quantity in biological bodies. The external field strength or incident power density corresponding to the limit for internal quantities is referred to as the reference level (RL) in the ICNIRP guidelines and exposure reference level in the IEEE standard. In the following discussion, we refer to the limit for external field strengths as RL, because it was defined as the maximum permissible exposure or reference level in the IEEE 2005 standard [3]. Even though the limits for the BR are identical in the guidelines/standard, the RLs differ by a factor of 12.9 for the magnetic field and 7.4 for the electric field in the intermediate frequencies ranging from 100 kHz to 100 MHz [1], [3].

In the IEEE standard, the limit for the RL from 100 kHz to 300 MHz has not been changed from the ANSI standard in 1982. In the ICNIRP guidelines, no apparent rationale for the limit was mentioned in the 1998 guidelines [1]. The SAR evaluation for the whole-body exposure became feasible after the late 1990s with the progress of computational resources and techniques (e.g., [4]). The limit for the RL should protect human even for the local SAR limit in addition to that for the whole-body averaged SAR. As the standard/guidelines were published before computation with anatomical human models was available, it is worth revisiting the relationship between the external field strength and local SARs as well as the whole-body averaged SAR, especially in the frequency range from 100 kHz to 10 MHz. Many studies have been conducted above 10 MHz (e.g., [5]–[9]), where the whole-body averaged SAR is important. However, the relationship between the external field strength and local SAR has not yet been evaluated in the frequency range down to 100 kHz. Only a few studies have discussed the local and whole-body SAR simultaneously, and this was above 10 MHz [8], [10], [11].

In the present study, the relationship of local and whole-body averaged SAR with external field strengths/incident power density is investigated in anatomical human body models using different computational methods. Intercomparison using various computational codes is also performed to confirm this relationship. For the first time, computational results with the full-wave analysis and quasi-static analysis are compared for whole-body exposures at intermediate frequencies. The extreme exposure scenarios, body models, and the postures were not considered considering the description in the draft version of the ICNIRP guidelines and IEEE standard.

II. METHODS

In the frequency range below approximately hundreds of kilohertz, the quasi-static approximation is often used without validation. In contrast, the full-wave analysis is often used at frequencies above 10 MHz. For uniform (plane-wave) exposures, no comparison has been performed in the frequency range considered here. These approaches have been compared in terms of local and whole-body averaged SARs for the first time. To investigate the differences between numerical approaches and different laboratories, three quasi-static and one full-wave analysis methods were considered.

A. QUASI-STATIC FINITE ELEMENT METHOD FOR ELECTRIC AND MAGNETIC FIELD EXPOSURES

The finite element method (FEM) with cubic elements [12] was used at Aalto University. Under the quasi-static assumption, the electric field in the body can be represented as

$$\mathbf{E} = -\nabla\phi - \frac{\partial \mathbf{A}_0}{\partial t}, \tag{1}$$

where ϕ is the electric scalar potential and $\mathbf{A_0}$ is the vector potential of the incident magnetic field. Owing to the continuity condition, the electric scalar potential in the body satisfies the following elliptical partial differential equation:

$$\nabla \cdot \sigma \nabla\phi = -\nabla \cdot \sigma \frac{\partial}{\partial t}\mathbf{A_0}, \tag{2}$$

with the boundary condition

$$\mathbf{n} \cdot \sigma(\nabla\phi + \frac{\partial}{\partial t}\mathbf{A_0}) = \frac{\partial}{\partial t}Q_s, \tag{3}$$

where σ is the conductivity and Q_s is the surface charge induced by the incident electric field.

For modeling the exposure to a magnetic field, Q_s was set to zero and $\mathbf{A_0}$ was calculated analytically. The exposure to an external electric field was modeled in two steps. First, the external electric potential in air was determined assuming that the body is a perfect electric conductor [13] by solving the following equation and boundary conditions:

$$\nabla \cdot \varepsilon_0 \nabla\phi_{ext} = 0, \tag{4}$$

$$\begin{cases} \mathbf{n} \cdot \nabla\phi_{ext} = -\mathbf{n} \cdot \mathbf{E_0}, & \text{on outer boundary} \\ \phi_{ext} = 0, & \text{on body surface,} \end{cases} \tag{5}$$

where $\mathbf{E_0}$ is the incident electric field and ε_0 is the permittivity of air. In (5), it is assumed that the outer boundary is at a sufficient distance so that the perturbation in the incident field owing to the body is negligible at the boundary.

Two nested grids [13] were used to numerically determine the external potential. The outer coarse grid had a resolution of 24 mm and a separation of at least 3.0 m between the body and the boundary of the computation domain. The body model was resized for the coarse grid. The boundary condition of the outer grid was set to a uniform electric field. The calculated electric field in the outer grid was interpolated and used to set the boundary condition of the inner grid, which had the same voxel resolution as the original body model. The distance of the boundary of the inner grid from the body was at least 12 cm. Finally, the induced charge Q_s in each voxel on the body surface was calculated from the normal component

of the external electric flux density, and the internal potential was determined by solving (2) and (3).

The electric scalar potential equations (2) and (4) were discretized using Galerkin FEM with piecewise linear basis functions. The elements were cubical, and the degrees of freedom were the values of the electric potential at the corners of each cube. This resulted in a sparse matrix equation for the unknown scalar potential values. The matrix equation was solved iteratively using the geometric multigrid method [12].

B. SCALAR POTENTIAL FINITE DIFERENCE METHOD

The scalar potential finite difference (SPFD) method [14] was used at Nagoya Institute of Technology (NITech) and South China Agricultural University (SCAU). The SPFD method sets the branch current instead of the loop current. The unknowns in this method are the scalar potential values at the nodes (corners) of each voxel. Branch currents flowing along the edges of the voxels are then derived from the potential difference between neighboring nodes and the conductivity of the voxels. The branch current calculation also takes into account magnetic vector potential of the applied magnetic field. By applying Kirchhoff's current law at all nodes, simultaneous equations are thereafter established. The potential is subsequently solved iteratively. The electric field along the side of the voxel is obtained by dividing the difference of the potentials between the nodes of the voxel by the distance across the nodes and then adding the vector potential.

$$\sum_{n=1}^{6} S_n \phi_n - \left(\sum_{n=1}^{6} S_n\right) \phi_0 = j\omega \sum_{n=1}^{6} (-1)^n S_n l_n A_{0n}, \quad (6)$$

where S_n, ϕ_n, l_n, ω, and A_{0n} denote the edge conductance derived from tissue conductivity, scalar potential, length between nodes, angular frequency, and magnetic vector potential, respectively. The matrix equations for SPFD were solved iteratively using the geometric multigrid method at NITech, similar to [12], and the Jacobi iterative method at SCAU [15].

C. Impedance Method

The impedance method [16] was used at the National Institute of Information and Communications Technology (NICT). In this method, an inhomogeneous human body is modeled as a three-dimensional complex impedance network. Each voxel is associated with permittivity and conductivity corresponding to the location in the human body model. As the impedance is assigned at each edge of the voxel, its values are determined by an average of the dielectric constants of four adjacent voxels, e.g., for the complex impedance along the x-direction:

$$\tilde{Z}_x\Big|_{i,j+\frac{1}{2},k+\frac{1}{2}} = \frac{1}{j\omega\varepsilon_0 \left(\tilde{\varepsilon}_r^a\big|_{i,j+\frac{1}{2},k+\frac{1}{2}}\right)} \frac{l_x}{l_y l_z}, \quad (7)$$

where ω and ε_0 are the angular frequency and free-space permittivity, respectively. l_x, l_y, and l_z are the edge lengths in the x-, y-, and z-directions, respectively. It should be noted that the impedance elements are locating on the edge of each voxel and, therefore, they reside on the locations $(i, j + 1/2, k + 1/2)$, $(i + 1/2, j, k + 1/2)$, and $(i + 1/2, j + 1/2, k)$ for the x-, y-, and z-direction, respectively, while the voxel center is located at (i, j, k). $\tilde{\varepsilon}_{\mathrm{r}}^{\mathrm{a}}$ denotes the complex relative permittivity averaged over four voxels cube in each direction, e.g., for the x-direction,

$$\tilde{\varepsilon}_r^a\big|_{i,j+\frac{1}{2},k+\frac{1}{2}} = \frac{\tilde{\varepsilon}_r|_{i,j,k} + \tilde{\varepsilon}_r|_{i,j+1,k} + \tilde{\varepsilon}_r|_{i,j,k+1} + \tilde{\varepsilon}_r|_{i,j+1,k+1}}{4}, \quad (8)$$

$$\tilde{\varepsilon}_r|_{i,j,k} = \left(\varepsilon_r - j\frac{\sigma}{\omega\varepsilon_0}\right)_{i,j,k}, \quad (9)$$

$\tilde{\varepsilon}_r$ denotes the complex relative permittivity. ε_{r} and σ are the relative permittivity and conductivity, respectively, associated with the voxel at the location indexes i, j, and k. Once the impedance network has been constructed, the induced loop currents at each voxel face are thereafter determined by applying an electromotive force according to Faraday's law and solving the system of equations using the successive over-relaxation method. After obtaining the loop currents, the line currents along the edges of each voxel can be calculated from the four loop currents surrounding each edge and the current at the center of each voxel is determined by averaging the four line-currents in each direction. Finally, the internal electric field is computed using the following equation, e.g., for the z-component electric field,

$$E_z^{in}\Big|_{i,j,k} = \frac{I_z^c\big|_{i,j,k}}{j\omega\varepsilon_0 \left(\varepsilon_r - j\frac{\sigma}{\omega\varepsilon_0}\right)_{i,j,k}} \frac{1}{l_x l_y}, \quad (10)$$

where $I_z^c|_{i,j,k}$ is the z-component current at the center of the voxel at the location indexes i, j, and k.

D. FINITE DIFFERENCE TIME DOMAIN METHOD

The finite-difference time-domain (FDTD) method [17] is used for full-wave analysis or plane-wave exposures. In this method, electric and magnetic fields are directly discretized in the time and space domains, respectively, and the central difference is used in the discretization process. The mesh is based on cubical cells. As the method is an explicit time-domain method, the matrix computation, which is usually complicated, is not required. Moreover, the method is suitable for parallel computing. The total-field/scattered-field formulation [17] was applied to generate an appropriate plane wave. The computational region was truncated by applying a thirty-layered convolutional perfectly matched layer absorbing boundary. The FDTD computation was conducted at Kitami Institute of Technology (KIT).

E. HUMAN BODY MODELS

To compute the variability of the SAR caused by the model morphology, five anatomic models were considered, including Japanese male and female models named TARO and

HANAKO, respectively (developed at NICT, Japan) [18]. These models were segmented into 51 tissue types. NORMAN, a normalized adult male model with 37 tissue types, was also used (developed at National Protection Agency (currently, Health New England), UK) [19]. Further, a European male model named Duke and a child model named Thelonious were used (developed at IT'IS Foundation, Switzerland) [20]. These models have over 70 tissue types. The resolution of each model was set to 2 mm. The height, weight, and number of tissues of these models are summarized in Table 1. The main feature of this study model selection is that the models that were developed at different research organizations were chosen. Three of the selected models are adult males with average body sizes, and thus, they can be used for studying the variability in between individuals of similar body sizes and the differences due to tissue segmentation. The models of an adult female and a three-year-old child were included to gain insight into the effects of body size on the SAR values. Note that the considered body models do not cover the entire population. For instance, models of very thin or obese people as well as models of infants or pregnant women were not included in the study.

TABLE 1. Parameters of anatomical human models.

Name	Height [m]	Weight [kg]	Number of Tissues
TARO	1.73	65	51
HANAKO	1.61	53	51
NORMAN	1.76	73	37
Duke	1.74	70	77
Thelonious	1.17	20	73

To incorporate the anatomically based model into the electromagnetic analysis, the electrical conductivity and dielectric constants of the tissues, which depend on the frequency, are required in magneto- and electro-quasi static analysis and full-wave analysis, respectively. These values were obtained from a formula based on the measurements in [21].

F. EXPOSURE SCENARIOS AND METRIC FOR EVALUATION

One of the models is chosen and assumed to stand in free space. Three sources of exposure were considered: uniform magnetic and electric fields and plane wave.

These three orientations of the magnetic fields that were considered are shown in Fig. 1. The definition of the directions is based on the Poynting vector for the plane wave. For electric or magnetic field exposures, only one component exists. Its direction is defined as the exposure direction.

For the electric field exposure and plane wave exposures, the electric field direction was chosen to be parallel to the human height direction. For the exposures, both free space and grounded conditions were considered. In the grounded conditions, the body models were assumed to stand on an infinite perfectly conducting ground plane. In the frequency range considered, the human body behaves like a small dipole/monopole, resulting in higher power absorption

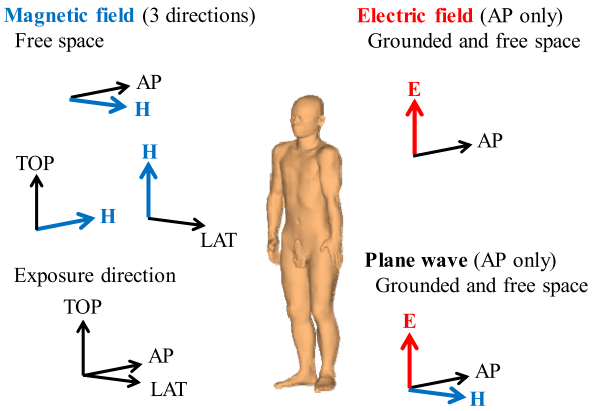

FIGURE 1. Orientation definition of magnetic, electric fields, and plane wave.

for standing postures. Although different exposure scenarios were discussed in previous studies [9], [22], [23], such scenarios were not considered in this study based on the public consultation version of the ICNIRP RF guidelines. Also, in the IEEE C95.1 draft standard, it was mentioned that there is no practical way to define a worst conceivable case.

The frequency range considered is to cover the frequency where the guidelines/standard specifies the limit in terms of the external field strength. In the ICNIRP guidelines, the limit for external field strength is prescribed from 0 Hz to 300 GHz, but for the thermal effect, it is greater than 100 kHz. The limit for the field strength is defined up to 100 MHz. Thus, our computation focuses in the frequency range from 100 kHz to 100 MHz.

The SAR can be defined as follows:

$$SAR = \frac{\sigma}{2\rho} |\mathbf{E}|^2 \tag{11}$$

where $|\mathbf{E}|$ [V/m] corresponds to the maximum value of the sinusoidal electric field, and ρ [kg/m^3] and σ [S/m] correspond to the density and conductivity of the tissue, respectively.

To calculate the SAR averaged over 10 g of contiguous tissue and 10 g of tissues in a cube shape were used as specified by the ICNIRP guidelines [1] and the IEEE C95.1-2005 standard [3], respectively. In [1] and [3], no detailed algorithm was prescribed. Thus, the algorithm developed by us following the C95.3-2002 standard [24] was used in this study. The whole-body averaged SAR is defined as the total power absorbed in the body model divided by the body weight (provided by the model developers). For grounded exposure scenarios, limb currents were also calculated in order to discuss the limit set in the guidelines [1].

At each frequency, the calculated whole-body or local SAR values were used to determine the maximal external magnetic/electric field strengths that satisfied the BRs. The obtained field strengths could then be directly compared with the RLs in the IEEE standard and ICNIRP guidelines.

In addition, for considering the variability of SARs between different laboratories (NITech, SCAU, NICT, and

Aalto), a reference value A_r is introduced as the mean value over the results obtained by the four research groups. The relative difference, D, between the reference value and the results calculated by either one of the groups is defined by the following expression:

$$D = \frac{A_i - A_r}{A_r}, \tag{12}$$

where the subscripts r and i correspond, respectively, to the data for the reference value and that obtained by the i-th group.

There is computational uncertainty in the grid (model) resolution at 2 mm. Using the FDTD method, the resolution of 2 mm was compared to 1 mm by Kühn *et al.* [8], who found that the uncertainty in the peak 10-g SAR was less than 0.25 dB (6%), calculated at 835 MHz and 2140 MHz. The uncertainty in WBA-SAR was smaller (0.1 dB, 2%). The uncertainty in the SAR due to grid size is known to further decrease at lower frequencies [25]. In the quasi-static computational methods, the iteration continues until the relative residual is less than 10^{-6}. The estimated error in the local electric field for this relative residual is less than 0.5% [12], and thus, its impact on the local and WBA-SAR may be ignored.

III. COMPUTATIONAL RESULTS

A. MAGNETIC FIELD EXPOSURE

Fig. 2 shows the SAR distributions in TARO for uniform magnetic field exposure with different exposure directions. The computational results obtained by NITech are plotted. The magnetic field strength was 1.0 A/m and the frequency was 10 MHz. As shown in Fig. 2, the SAR distributions were different for different field directions. The *in situ* electric field is induced by the magnetic field based on Faraday's law, which assumes that the human body is a poor conductor.

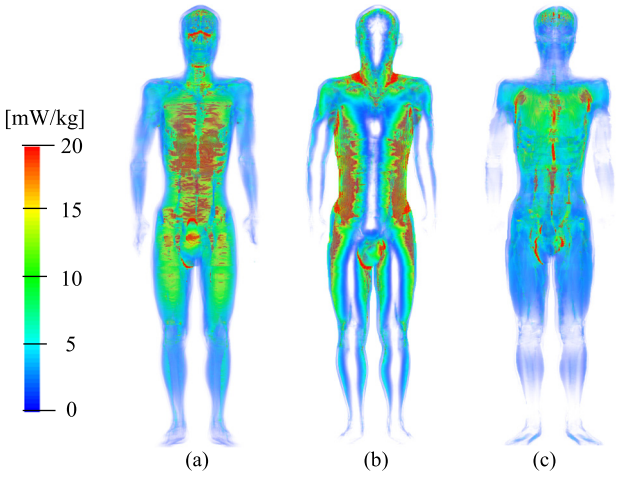

FIGURE 2. SAR distributions in TARO (Japanese adult male model) standing in free space for magnetic field exposure at 10 MHz. Exposure directions are (a) LAT, (b) AP, and (c) TOP.

The field strength becomes the maximum around the model surface (see AP exposure as an example).

The frequency dependence of the external field satisfying the local peak and whole-body SAR limits is computed for a uniform magnetic field in the frequency range from 100 kHz to 100 MHz. In the magneto-quasi-static regime, the ground plane or metallic object does not perturb the external field distribution, and thus, the human model is placed in free space. As shown in Fig. 3 (a) and (b), the whole-body and local SARs computed by NITech satisfied the limit prescribed in the IEEE standard [3] and ICNIRP guidelines [1], [26]. The whole-body SAR was more restrictive than local SAR, though were comparable in the AP direction.

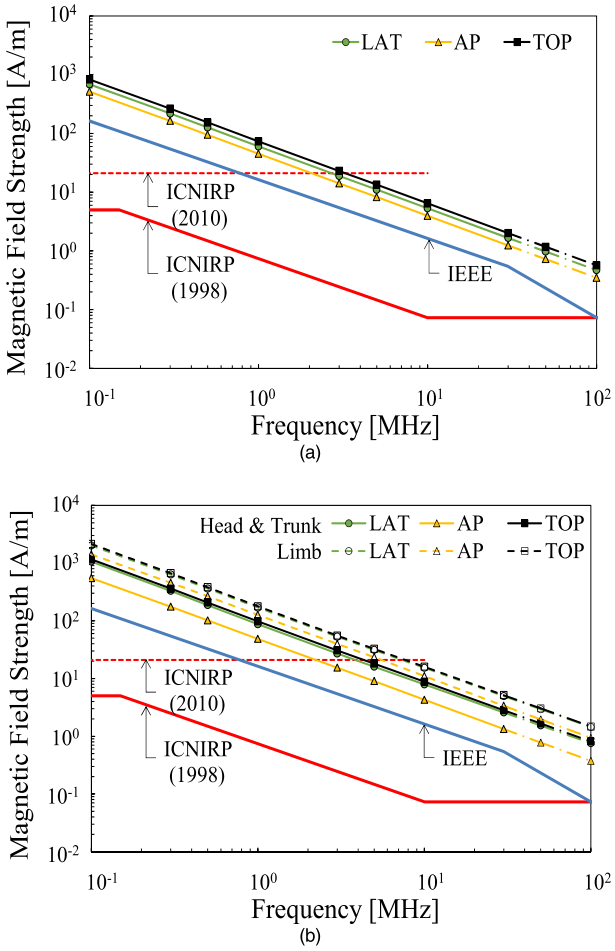

FIGURE 3. Frequency dependence of the magnetic field strength satisfying the basic restrictions for (a) whole-body SAR and (b) local SAR averaged over 10 g of tissue in TARO for a uniform magnetic field exposure.

The worst case for TARO is in the AP direction (Fig. 3). The variability of SARs in the different models is computed as shown in Fig. 4 for AP magnetic field exposure. As shown in Fig. 4, the whole-body averaged SAR increases for models with larger height and weight (see Table 1). The SAR in the child model was much smaller than that in the adult.

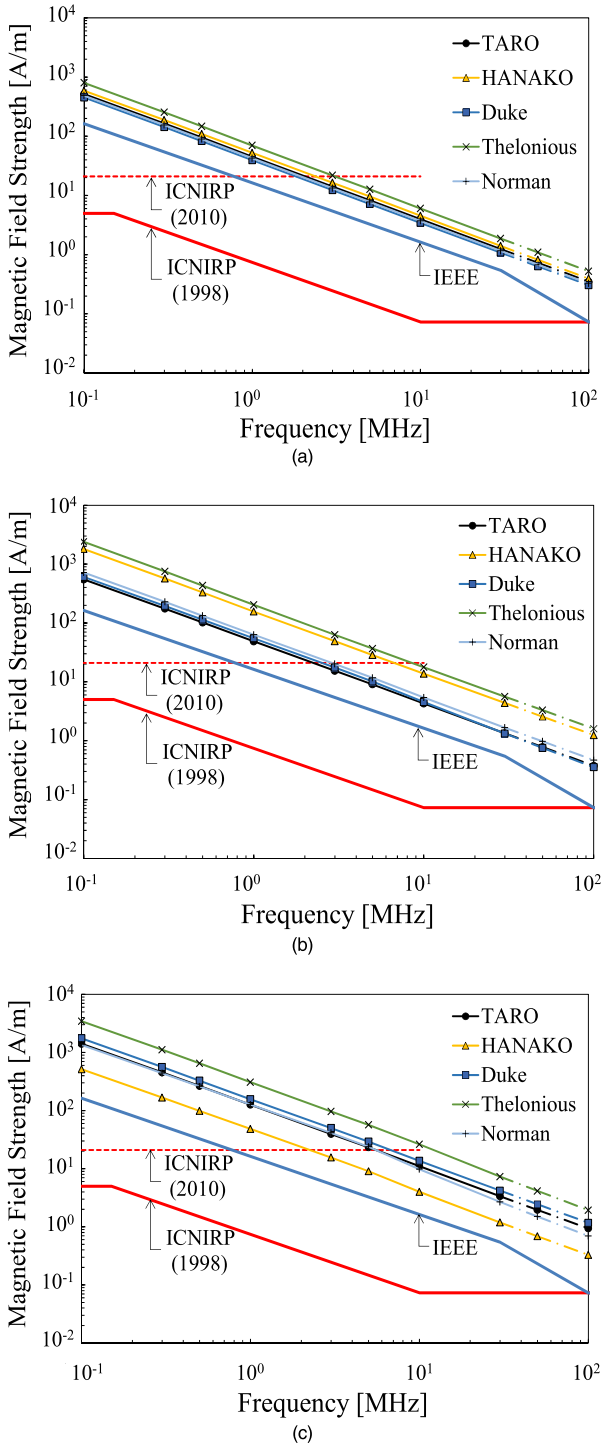

FIGURE 4. Frequency dependence of magnetic field strength satisfying the basic restrictions for (a) whole-body SAR, (b) local SAR (Head & Trunk), and (c) local SAR (Limb) in various human models for magnetic field exposure in the AP direction.

Moreover, in all the models except for Thelonious, the worst exposure direction was in the AP direction.

To analyze the results obtained by different groups, the relative difference D for the SAR in TARO for a uniform magnetic field exposure of three directions at 0.1, 10 and 100 MHz is listed in Table 2. Also, Table 2 lists the comparison of the results in the Duke model for magnetic field exposure in the AP direction to consider the effect of different anatomical model. The maximal relative difference was 25.1%, which was observed for the local SAR (Head & Trunk) at 100 MHz in the AP direction (computed at NICT). This difference might be attributed to the differences in the computational methods; the influence of the displacement current was considered by NICT using complex conductivity (See Sec. II. C). This is also supported by the fact that the difference is the largest for the AP exposure direction where the body dimension effect is largest [35]. In addition,

TABLE 2. Differences (D, %) of SAR values in TARO for uniform magnetic field (1 A/m) exposure at 0.1, 10 and 100 MHz. Models and exposure directions: (a): TARO(LAT), (b) TARO(AP), (c) TARO(TOP), (d) Duke(AP).

(a)

	Freq. [MHz]	NIT	SCAU	NICT	Aalto
WBA-SAR	0.1	0.5	-6.8	-0.3	6.7
	10	-2.8	-8.0	2.6	8.2
	100	-2.0	-7.2	4.8	4.4
Local-SAR (Head&Trunk)	0.1	0.0	3.8	-1.8	-2.1
	10	-0.4	2.5	-1.4	-0.7
	100	-1.9	1.1	1.4	-0.6
Local-SAR (Limb)	0.1	0.8	-6.4	2.7	2.8
	10	1.2	-5.2	1.4	2.6
	100	-0.4	-6.3	5.0	1.8

(b)

	Freq. [MHz]	NIT	SCAU	NICT	Aalto
WBA-SAR	0.1	0.4	-8.1	1.3	6.5
	10	-4.7	-11.2	8.8	7.1
	100	-2.8	-9.3	5.8	6.3
Local-SAR (Head&Trunk)	0.1	11.2	3.7	2.2	-17.1
	10	10.9	0.8	8.6	-20.3
	100	25.0	14.9	-25.1	-14.9
Local-SAR (Limb)	0.1	-0.4	-1.0	2.9	-1.5
	10	-2.4	-4.8	1.2	6.0
	100	4.7	2.3	-3.0	-4.0

(c)

	Freq. [MHz]	NIT	SCAU	NICT	Aalto
WBA-SAR	0.1	-0.5	-8.9	1.1	8.4
	10	-3.6	-10.4	3.7	10.3
	100	-2.2	-8.8	4.2	6.8
Local-SAR (Head&Trunk)	0.1	-12.0	2.9	0.8	8.3
	10	-13.2	7.7	-3.4	8.8
	100	-6.3	8.5	-12.8	10.6
Local-SAR (Limb)	0.1	4.8	6.6	9.7	-21.1
	10	5.0	6.5	6.7	-18.2
	100	7.9	9.9	-2.7	-15.0

(d)

	Freq. [MHz]	NIT	SCAU	NICT	Aalto
WBA-SAR	0.1	2.6	-3.9	-5.6	7.0
	10	-2.9	-7.5	0.6	9.8
	100	2.3	-2.4	-10.3	10.4
Local-SAR (Head&Trunk)	0.1	-3.5	-18.8	19.3	3.0
	10	-0.1	-19.6	7.1	12.6
	100	22.3	-9.4	-10.7	-2.1
Local-SAR (Limb)	0.1	-9.6	0.7	8.2	0.7
	10	-5.9	-1.4	2.3	5.0
	100	3.9	10.6	-20.6	6.1

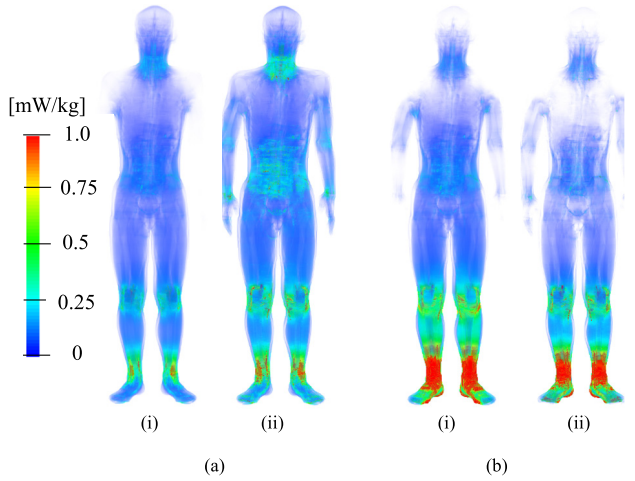

FIGURE 5. SAR distributions in the TARO model in (a) free space at 60 MHz and (b) grounded at 30 MHz for (i) electric field (1 V/m) and (ii) plane wave (1/120 π W/m^2) exposure.

the mean relative difference by four groups was 5.4%, 6.2% and 7.5% at 100 kHz, 10 MHz and 100 MHz, respectively, suggesting that the displacement current effect becomes large with the increase of the frequency.

B. ELECTRIC FIELD AND PLANE-WAVE EXPOSURES

The effects of electric field and plane-wave exposures were examined by Aalto and KIT, respectively. The plane wave occurred from the AP direction and the electric field was in the TOP direction (Fig. 1). Figs. 5 (a) and (b) show the SAR distributions in the Japanese male adult in free space at 60 MHz and that grounded at 30 MHz for electric field and plane-wave exposures. As shown in Fig. 5, the local SAR shows a peak around the ankle for both of the cases, which is attributable to its small cross-sectional area. The distributions for electric field and plane-wave exposure are similar to each other, suggesting that the SAR is mainly caused by the electric field.

Fig. 6 (a) and (b) show the frequency dependence of the whole-body and local SAR in the human standing in free space and in the grounded plane from 100 kHz–100 MHz. The results of the Duke in [10] and the TARO in [11] are also presented, which are in good agreement with our results obtained in this study. As shown in Fig. 6 (a), the whole-body SAR is a more restrictive factor to set the RL in free space, but not for the grounded case, especially below 30 MHz where the SAR in the limb becomes more restrictive (Fig. 6 (b)).

As shown in Fig. 7, the comparison of the whole-body averaged SAR between the plane-wave and electric field was at most 10% below 30 MHz for the human standing in free space and 10 MHz in grounded cases. These frequencies are the upper limits of validity for the quasi-static approximation. The violation of the quasi-static assumption is also visible in Fig. 6, where the curve for quasi-static approximation crosses the RL around 60 MHz and 30 MHz. On the contrary, this phenomenon is not observed for the plane-wave exposure. The contribution of the magnetic field,

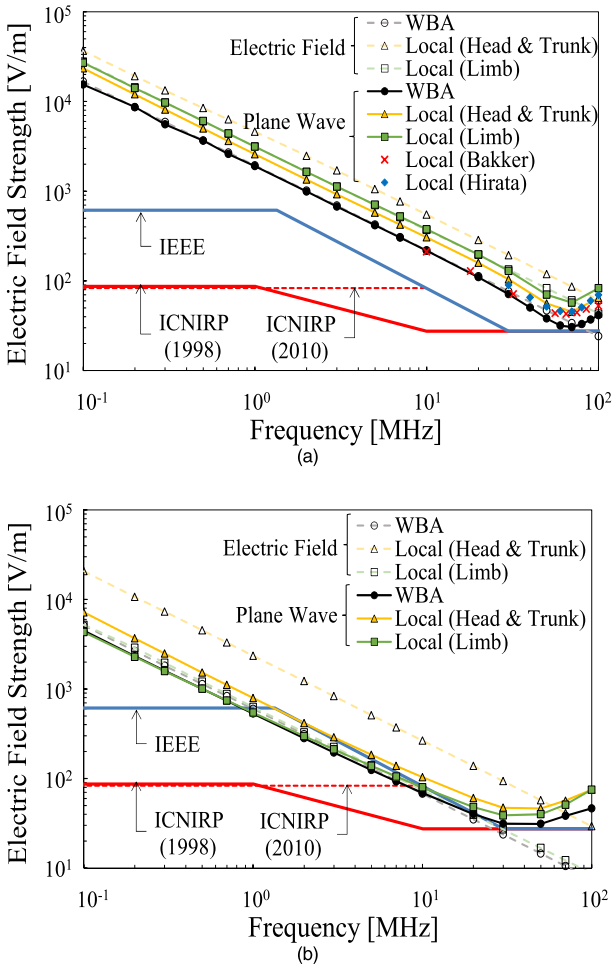

FIGURE 6. Frequency dependence of electric field strength satisfying the basic restrictions for the whole-body and local SARs in the TARO model standing in (a) free space and (b) grounded plane.

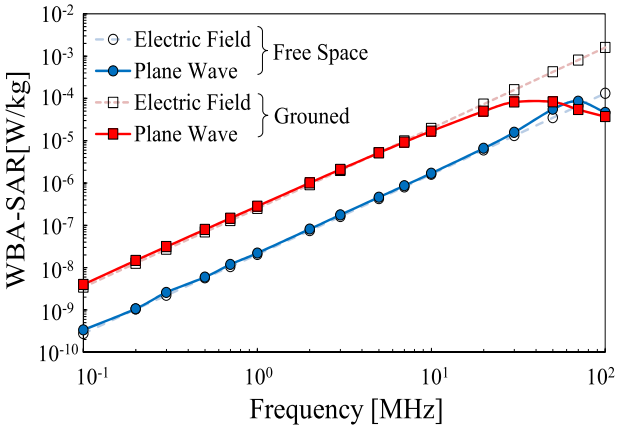

FIGURE 7. Difference of the whole-body averaged SAR in free space and grounded between electric field and plane-wave exposures.

corresponding to the plane wave, was at most 1%, (not shown here). This difference thus suggests that the contribution of the electric field is predominant for exposure in this frequency range (parallel to the human height direction).

Fig. 8 shows the variability of the whole-body average and peak 10-g SARs in different models for electric field and plane-wave exposures. As shown in Fig. 8 (a), the curve of the whole-body-averaged SAR has a bottom at approximately 30 MHz. The violation of RL to the computed whole-body averaged SAR was observed below 30 MHz in the IEEE standard.

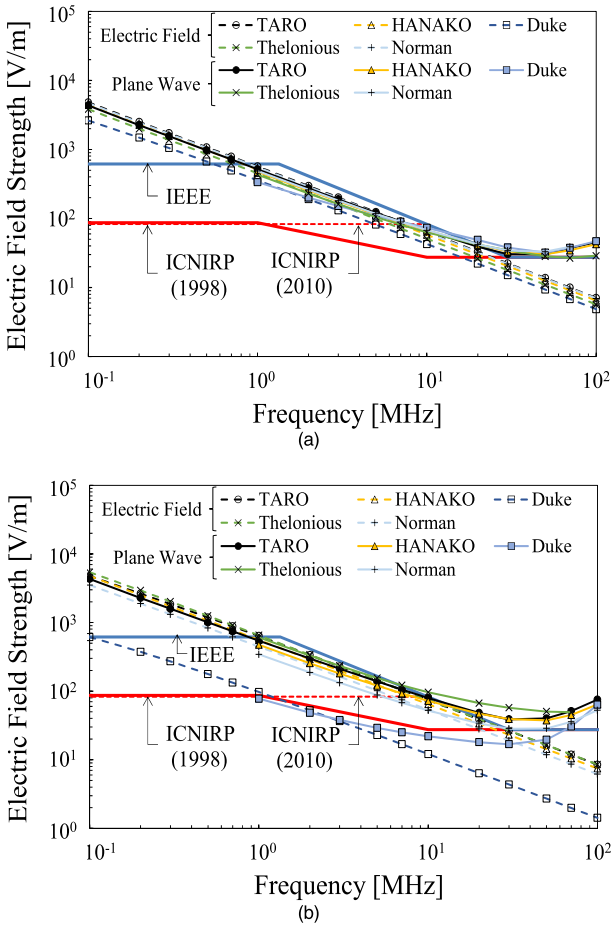

FIGURE 8. Frequency dependence of electric field strength satisfying the basic restrictions for (a) whole-body average and (b) peak 10-g average SARs. Grounded conditions are assumed.

As shown in Fig. 8 (b), the curve of the local 10-g SAR has a bottom at approximately 30 MHz. However, in the Duke model, the bottom appeared at approximately 30 MHz and the slope below that frequency was different from the others. This is attributable to the contact condition of the sole; peak 10-g SAR appeared around the thumb toe. In other models, it was observed around and above the ankle. Except in this model, the discrepancy was minor at approximately 30 MHz and some discrepancy below 30 MHz was observed, as in Figs. 8 (a) and (b).

Fig. 9 shows the limb current required for 2 W/kg of local 10-g SAR. As shown in Fig. 9, discrepancy was observed only for the Duke model, as discussed in the results of the peak 10-g SAR in the ankle.

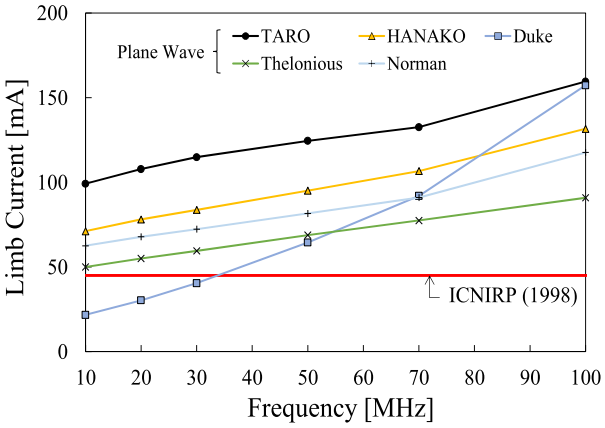

FIGURE 9. Limb current corresponding to the limit (4 W/kg)of the peak 10-g average SAR in the ICNIRP guidelines, 1998.

IV. DISCUSSION

For magnetic field exposure, the whole-body averaged and local SARs were computed at frequencies below 100 MHz (see Fig. 3). We thereafter observed that the whole-body averaged and peak 10-g averaged SARs were below their corresponding BRs for exposure at the amplitude of the RL; it was the first confirmation that the RL can warrant simultaneously local and whole-body averaged SAR BR at frequencies from 100 kHz to 10 MHz. The worst case for the local SAR is the exposure in the AP direction, which is consistent with the tendency at low frequencies ($<$ 100 kHz) where the nerve stimulation is dominant [27]. Note that in the regime where electrostimulation is dominant, the physical quantity for BR is the internal electric field strength averaged over a 2-mm cube in ICNIRP [1] and 5-mm line segment in IEEE [2], and thus, direct comparison is not feasible.

From Fig. 4, the variability of the whole-body averaged and peak 10-g averaged SARs is consistent with that at low frequencies; the SARs have a tendency to be higher in the models with larger sizes. One reason for this is that, by Faraday's law, a larger cross-sectional area of the body produces a larger induced field [28]. However, this is not always true as also shown in [11], where the local SAR in the child model was larger than in the adult models in some cases. This can be attributable to the model inhomogeneity. As shown in [11], the position where peak local SAR appears are different. Similarly, for low-frequency uniform exposures, the *in situ* electric field of 2-mm cube in the large and fatty model was not always larger than that in typical adult models [29].

The computational difference between groups is confirmed to be less than approximately 25% in the local SAR and 10% in the whole-body averaged SAR, which is consistent with a previous intercomparison for an *in situ* electric field [30] ($<$ 10 % in peak internal electric field) and a local SAR for exposure from handset antennas [31] ($<$ 30%). The SAR is proportional to the square of the electric field and thus the differences in the intercomparison at LF and IF are consistent. This difference may support the description of the public

consultation version of the ICNIRP guidelines that dosimetric uncertainty associated with deriving exposure values can be included in the reduction factor. Also note that this is included in the safety factor in the draft IEEE standard. In the LF dosimetry, NITech and Aalto University conducted the intercomparison of voxel internal electric fields in different models. Then, the uncertainty in the dosimetry was comparable for different exposure directions [32].

As shown in Figs. 6 and 8, local and whole-body averaged SARs were also computed for exposure to electric fields to confirm the relationship between BR and RL. From computational results of the local SAR in free space, the relationship between BR and RL was satisfied; it was substantially conservative for the ICNIRP guidelines and had a slight excess below 40 MHz for the IEEE C95.1 standard. Instead, the whole-body averaged SAR in the child model exceeds the reference level by 30%, which is consistent with the previous studies [4], [6]–[9], [33]. Moreover, in some of the models, local SARs in the ankle are not satisfied for the grounded models. As mentioned in the results section, the SAR around the ankle largely depends on the contact condition of the ground and sole; in the Duke model, only a few voxels contact the ground, resulting in locally high SAR value only in that area. Such computational results using special grounded conditions may not be appropriate for guideline setting, though it is worth presenting them here to know the physical phenomena in the dosimetry. For example, in the low-frequency dosimetry, computational uncertainty is extensively discussed [34].

The maximum frequency where the quasi-static approximation is valid is specified below approximately 10 MHz for grounded humans and 30 MHz for humans standing in free space. This regime has been clarified for uniform field exposures by using both full-wave and quasi-static approaches. The conditions for quasi-static approximation are: (i) the body length is much shorter than both the free space wavelength and the skin depth, and (ii) the conduction currents dominate the displacement current [35]. The effect of the displacement current is approximately 10% in brain tissue and skin at 10 MHz. The frequencies specified above are approximately a half of the resonance frequency (10 MHz and 30 MHz in ground and in free space), and thus, the limiting factor of quasi-static would be the body height. The tendency was similar to the discussion on effectiveness of quasi-static approximation for non-uniform field exposures from a wireless power transfer system [36].

Notably, grounding of a human body might not occur in realistic exposure scenarios. Possible scenarios corresponding to the grounded human would be a human wearing shoes with conducting rubber soles, and a human with wet shoes standing on wet ground. The latter case may represent the intermediate situation of the free space and grounded cases. As shown in Fig. 5, the ankle SAR becomes significant both for grounded and in free space. Once ungrounded, the RL in the IEEE and ICNIRP would be well satisfied for electric and plane-wave exposures. Similar discussion can be found on whole-body averaged SAR in grounded humans at higher frequencies [37]–[39].

In the ICNIRP guidelines and IEEE standard, the compliance with the reference level in the limb current becomes essential when the field uniformity is high, which is designated for local SAR compliance. The corresponding limit for the limb current is 45 mA for the general public. If this limit is applied simultaneously, the local and whole-body averaged SARs are well satisfied. In realistic exposure scenarios, the field strength averaged over the volume where the human exists is non-uniform, and thus, limb current assessment around the ankle becomes essential for grounded humans or similar cases.

Only typical human body models were considered in this study. In addition to the body model morphology, additional factors, including dielectric properties of tissue and model postures, should be considered. As mentioned in the IEEE C95.1 draft standard, the uncertainties in computational models and those in dosimetry have been included in the safety factor. To further investigate variability of SAR, the validation of measurement on SAR and parameters related to the SAR, especially for human volunteer studies, would be needed (e.g., [40], [41]).

V. CONCLUSIONS

In this study, we conducted intercomparison of internal physical quantities for human model exposure to an electromagnetic field in the intermediate frequency (mainly from 100 kHz to 10 MHz). The feature of this intercomparison was that different computational approximations, i.e., quasi-static approximation and full-wave analysis, were applied. The maximum frequency where the quasi-static approximation is valid is specified below approximately 10 MHz for grounded humans and 30 MHz for humans standing in free space. Subsequently, we derived the relationship between local SARs and external field strength from 100 kHz to 100 MHz. Especially, the SARs for the exposure to the magnetic field from 100 kHz to 10 MHz and the local SARs in the limb grounded case have not been previously reported. We thereafter suggested that the reference level in the ICNIRP is very conservative at frequencies below 30 MHz whereas some marginal discrepancy exists in the IEEE C95.1. Another finding was that the local SARs are generally satisfied even for the RL designed for whole-body averaged SARs both for magnetic and electric fields. The results obtained here would be useful when revising and harmonizing the difference of reference levels set by ICNIRP and IEEE.

ACKNOWLEDGMENT

The authors would like to thank Dr. Kari Jokela (retired, Finland) and Dr. Soichi Watanabe (National Institute of Information and Communications Technology, Japan). This study was conducted in part as an activity of IEEE International Committee on Electromagnetic Safety Technical Committee 95, Subcommittee 6, Task Force 1 (Chair: Tatsuya Kashiwa, Secretary: Kenji Taguchi).

REFERENCES

[1] A. Ahlbom *et al.*, "Guidelines for limiting exposure to time-varying electric, magnetic, and electromagnetic fields (up to 300 GHz)," *Health Phys.*, vol. 74, no. 4, pp. 494–521, 1998.

[2] *IEEE Standard for Safety Levels With Respect to Human Exposure to Radio Frequency Electromagnetic Fields, 3 kHz to 300 GHz*, IEEE Standard-C95.6, 2002.

[3] *IEEE Standard for Safety Levels With Respect to Human Exposure to Radio Frequency Electromagnetic Fields, 3 kHz to 300 GHz*, IEEE Standard-C95.1, 2005.

[4] P. J. Dimbylow, "Fine resolution calculations of SAR in the human body for frequencies up to 3 GHz," *Phys. Med. Biol.*, vol. 47, no. 16, pp. 2835–2846, 2002.

[5] P. Dimbylow and W. Bolch, "Whole-body-averaged SAR from 50 MHz to 4 GHz in the University of Florida child voxel phantoms," *Phys. Med. Biol.*, vol. 52, no. 22, pp. 6639–6649, 2007.

[6] A. Hirata, S. Kodera, J. Wang, and O. Fujiwara, "Dominant factors influencing whole-body average SAR due to far-field exposure in whole-body resonance frequency and GHz regions," *Bioelectromagnetics*, vol. 28, pp. 484–487, Sep. 2007.

[7] E. Conil, A. Hadjem, F. Lacroux, M. F. Wong, and J. Wiart, "Variability analysis of SAR from 20 MHz to 2.4 GHz for different adult and child models using finite-difference time-domain," *Phys. Med. Biol.*, vol. 53, no. 6, pp. 1511–1525, 2008.

[8] S. Kühn, W. Jennings, A. Christ, and N. Kuster, "Assessment of induced radio-frequency electromagnetic fields in various anatomical human body models," *Phys. Med. Biol.*, vol. 54, no. 4, p. 875, 2009.

[9] T. Uusitupa, I. Laakso, S. Ilvonen, and K. Nikoskinen, "SAR variation study from 300 to 5000 MHz for 15 voxel models including different postures," *Phys. Med. Biol.*, vol. 55, no. 4, p. 1157, 2010.

[10] J. F. Bakker, M. M. Paulides, A. Christ, N. Kuster, and G. C. van Rhoon, "Assessment of induced SAR in children exposed to electromagnetic plane waves between 10 MHz and 5.6 GHz," *Phys. Med. Biol.*, vol. 55, no. 11, p. 3115, 2010.

[11] K. Wake *et al.*, "Derivation of coupling factors for different wireless power transfer systems: Inter- and intralaboratory comparison," *IEEE Trans. Electromagn. Compat.*, vol. 59, no. 2, pp. 677–685, Apr. 2017.

[12] I. Laakso and A. Hirata, "Fast multigrid-based computation of the induced electric field for transcranial magnetic stimulation," *Phys. Med. Biol.*, vol. 57, no. 23, pp. 7753–7765, 2012.

[13] P. J. Dimbylow, "Current densities in a 2 mm resolution anatomically realistic model of the body induced by low frequency electric fields," *Phys. Med. Biol.*, vol. 45, no. 4, p. 1013, 2000.

[14] Z. Sienkiewicz, E. van Rongen, R. Croft, G. Ziegelberger, and B. Veyret, "A closer look at the thresholds of thermal damage: Workshop report by an ICNIRP Task Group," *Health Phys.*, vol. 111, no. 3, pp. 300–306, 2016.

[15] Y. Diao, W. N. Sun, Y. Q. He, S. W. Leung, and Y. M. Siu, "Equivalent magnetic vector potential model for low-frequency magnetic exposure assessment," *Phys. Med. Biol.*, vol. 62, no. 19, p. 7905, 2017.

[16] N. Orcutt and O. P. Gandhi, "A 3-D impedance method to calculate power deposition in biological bodies subjected to time varying magnetic fields," *IEEE Trans. Biomed. Eng.*, vol. BME-35, no. 8, pp. 577–583, Aug. 1988.

[17] A. Taflove and S. Hagness, *Computational Electrodynamics: The Finite-Difference Time-Domain Method*, 3rd ed. Norwood, MA, USA: Artech House, 2003.

[18] T. Nagaoka *et al.*, "Development of realistic high-resolution whole-body voxel models of Japanese adult males and females of average height and weight, and application of models to radio-frequency electromagnetic-field dosimetry," *Phys. Med. Biol.*, vol. 49, no. 1, pp. 1–15, 2004.

[19] P. J. Dimbylow, "FDTD calculations of the whole-body averaged SAR in an anatomically realistic voxel model of the human body from 1 MHz to 1 GHz," *Phys. Med. Biol.*, vol. 42, no. 3, pp. 479–490, 1997.

[20] A. Christ *et al.*, "The virtual family—Development of surface-based anatomical models of two adults and two children for dosimetric simulations," *Phys. Med. Biol.*, vol. 55, pp. N23–N38, Dec. 2010.

[21] S. Gabriel, R. W. Lau, and C. Gabriel, "The dielectric properties of biological tissues: III. Parametric models for the dielectric spectrum of tissues," *Phys. Med. Biol.*, vol. 41, no. 11, pp. 2271–2293, 1996.

[22] R. P. Findlay and P. J. Dimbylow, "Effects of posture on FDTD calculations of specific absorption rate in a voxel model of the human body," *Phys. Med. Biol.*, vol. 50, p. 3825, Jul. 2005.

[23] T. Nagaoka and S. Watanabe, "Voxel-based variable posture models of human anatomy," *Proc. IEEE*, vol. 97, no. 12, pp. 2015–2025, Dec. 2009.

[24] *IEEE Recommended Practice for Measurements and Computations of Radio Frequency Electromagnetic Fields With Respect to Human Exposure to Such Fields, 100 kHz-300 GHz*, IEEE Standard C95.3-2002, 2002.

[25] P. Dimbylow, W. Bolch, and C. Lee, "SAR calculations from 20 MHz to 6 GHz in the University of Florida newborn voxel phantom and their implications for dosimetry," *Phys. Med. Biol.*, vol. 55, p. 1519, Feb. 2010.

[26] International Commission on Non-Ionizing Radiation Protection, "Guidelines for limiting exposure to time-varying electric and magnetic fields (1 Hz to 100 kHz)," *Health Phys.*, vol. 99, no. 6, pp. 818–836, 2010.

[27] M. A. Stuchly and T. W. Dawson, "Interaction of low-frequency electric and magnetic fields with the human body," *Proc. IEEE*, vol. 88, no. 5, pp. 643–664, May 2000.

[28] R. Kavet, T. Dovan, and J. P. Reilly, "The relationship between anatomically correct electric and magnetic field dosimetry and published electric and magnetic field exposure limits," *Radiat. Protection Dosimetry*, vol. 152, pp. 279–295, May 2012.

[29] X.-L. Chen *et al.*, "Analysis of human brain exposure to low-frequency magnetic fields: A numerical assessment of spatially averaged electric fields and exposure limits," *Bioelectromagnetics*, vol. 34, no. 5, pp. 375–384, Jul. 2013.

[30] A. Hirata *et al.*, "Intercomparison of induced fields in Japanese male model for ELF magnetic field exposures: Effect of different computational methods and codes," *Radiat. Protection Dosimetry*, vol. 138, no. 3, pp. 237–244, 2010.

[31] B. B. Beard *et al.*, "Comparisons of computed mobile phone induced SAR in the SAM phantom to that in anatomically correct models of the human head," *IEEE Trans. Electromagn. Compat.*, vol. 48, no. 2, pp. 397–407, May 2006.

[32] K. Aga, A. Hirata, and I. Laakso, "Intercomparison of *in-situ* electric field in human models for uniform magnetic field exposures," in *Proc. Eur. EMC*, Amsterdam, The Netherlands, 2018, pp. 515–520.

[33] J. Wang, O. Fujiwara, S. Kodera, and S. Watanabe, "FDTD calculation of whole-body average SAR in adult and child models for frequencies from 30 MHz to 3 GHz," *Phys. Med. Biol.*, vol. 51, no. 17, pp. 4119–4127, 2006.

[34] J. P. Reilly and A. Hirata, "Low-frequency electrical dosimetry: Research agenda of the IEEE International Committee on Electromagnetic Safety," *Phys. Med. Biol.*, vol. 61, no. 12, p. R138, 2016.

[35] T. W. Dawson, J. De Moerloose, and M. A. Stuchly, "Comparison of magnetically induced ELF fields in humans computed by FDTD and scalar potential FD codes," *Appl. Comput. Electromagn. Soc. J.*, vol. 11, pp. 63–71, Nov. 1996.

[36] A. Hirata, F. Ito, and I. Laakso, "Confirmation of quasi-static approximation in SAR evaluation for a wireless power transfer system," *Phys. Med. Biol.*, vol. 58, no. 17, p. N241, 2013.

[37] A. Hirata *et al.*, "Estimation of the whole-body averaged SAR of grounded human models for plane wave exposure at respective resonance frequencies," *Phys. Med. Biol.*, vol. 57, no. 24, p. 8427, 2012.

[38] B. Kibret, A. K. Teshome, and D. T. H. Lai, "Cylindrical antenna theory for the analysis of whole-body averaged specific absorption rate," *IEEE Trans. Antennas Propag.*, vol. 63, no. 11, pp. 5224–5229, Nov. 2015.

[39] D. Poljak, C. Y. Tham, O. Gandhi, and A. Sarolic, "Human equivalent antenna model for transient electromagnetic radiation exposure," *IEEE Trans. Electromagn. Compat.*, vol. 45, no. 1, pp. 141–145, Feb. 2003.

[40] I. D. Flintoft, M. P. Robinson, G. C. R. Melia, A. C. Marvin, and J. F. Dawson, "Average absorption cross-section of the human body measured at 1–12 GHz in a reverberant chamber: Results of a human volunteer study," *Phys. Med. Biol.*, vol. 59, no. 13, p. 3297, 2014.

[41] J. Wang, T. Suzuki, O. Fujiwara, and K. Harima, "Measurement and validation of GHz-band whole-body average SAR in a human volunteer using reverberation chamber," *Phys. Med. Biol.*, vol. 57, no. 23, p. 7893, 2012.

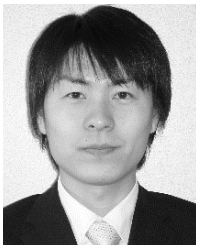

KENJI TAGUCHI received the B.E., M.E., and Ph.D. degrees in electrical and electronic engineering from the Kitami Institute of Technology, Kitami, Japan, in 2001, 2003, and 2006, respectively.

From 2006 to 2009, he joined the Department of Information and Communication Engineering, Kumamoto National College of Technology, as an Assistant Professor. Since 2009, he has been an Associate Professor with the Department of Electrical and Electronic Engineering, Kitami Institute of Technology. His research interests include the analysis of electromagnetic fields, electromagnetic compatibility, and optimization problems. He is a Secretary of Task Force under EMF Dosimetry Modeling of IEEE International Committee on Electromagnetic Safety.

ILKKA LAAKSO (M'14) received the M.Sc. (Tech.) degree in electromagnetics from the Helsinki University of Technology, Espoo, Finland, in 2007, and the D.Sc. (Tech.) degree in electromagnetics from Aalto University, Espoo, in 2011.

From 2013 to 2015, he was a Research Assistant Professor and a Research Associate Professor with the Department of Computer Science and Engineering, Nagoya Institute of Technology. Since 2015, he has been an Assistant Professor in electromagnetics in health technologies with Aalto University. He has authored more than 80 papers published in international journals and conference proceedings. His current research focuses on computational bioelectromagnetic modeling for assessment of human safety and biomedical applications. He was a recipient of several awards, including the Student Award in International Symposium on EMC, Kyoto, in 2009; the Ericsson Young Scientist Award, in 2011; and the Young Scientist Award in URSI General Assembly and Scientific Symposium, Montreal, QC, Canada, in 2017. He is the Secretary and a Working Group Chair of subcommittee of EMF Dosimetry Modeling of IEEE International Committee on Electromagnetic Safety and a member of the Scientific Expert Group of the International Commission on Non-Ionizing Radiation Protection.

KATSUAKI AGA received the B.E. degree in electrical and computer engineering from the National Institute of Technology, Kagawa College, Japan, in 2017. He is currently pursuing the master's degree in electrical and mechanical engineering with the Nagoya Institute of Technology, Nagoya, Japan.

His current research focuses on human protection from electromagnetic field at low and intermediate frequency.

AKIMASA HIRATA (S'98–M'01–SM'10–F'17) received the B.E., M.E., and Ph.D. degrees in communications engineering from Osaka University, Suita, Japan, in 1996, 1998, and 2000, respectively.

From 1999 to 2001, he was a Research Fellow of the Japan Society for the Promotion of Science, and also a Visiting Research Scientist at the University of Victoria, Victoria, BC, Canada, in 2000. In 2001, he joined the Department of Communications Engineering, Osaka University, as an Assistant Professor. In 2004, he joined, as an Associate Professor, the Department of Computer Science and Engineering, Nagoya Institute of Technology, where he is currently a Full Professor (Director, Research Center for Bioelectromagnetic Engineering). His research interests include electromagnetics and thermodynamics in biological tissue, waveguide analysis, EMC and EMI, and computational techniques in electromagnetics. He is a fellow of the Institute of Physics, and a member of IEICE, IEE Japan, and Bioelectromagnetics Society. He is an editorial board member of physics in medicine and biology, a member of the main commission and a Chair of project group of International Commission on Non-Ionizing Radiation Protection, and a member of administrative committee and a Subcommittee (EMF Dosimetry Modeling) Chair of IEEE International Committee on Electromagnetic Safety, and an Expert of World Health Organization. He was a recipient of several awards, including the Young Scientists' Prize (2006) and the Prizes for Science and Technology (Research Category 2011, Public Understanding Promotion Category 2014) by the Commendation for Science and Technology by the Minister of Education, Culture, Sports, Science, and Technology, Japan, and the IEEE EMC-S Technical Achievement Award (2015), and the Japan Academy Medal / JSPS Prize (2018). From 2006 to 2012, he was also an Associate Editor of the IEEE Transactions on Biomedical Engineering.

YINLIANG DIAO (M'17) received the B.E. degree from Chongqing University, Chongqing, China, in 2008, the M.S. degree in electronic engineering from the Beijing University of Posts and Telecommunications, Beijing China, in 2011, and the Ph.D. degree in electronic engineering from the City University of Hong Kong, Hong Kong, in 2016. In 2017, he joined South China Agricultural University, Guangzhou, China, as an Assistant Professor.

His research interests include human safety issues in electromagnetic compatibility and bioelectromagnetics.

JERDVISANOP CHAKAROTHAI (S'06–M'10) received the B.E. degree in electrical and electronic engineering from Akita University, Akita, Japan, in 2003, and the M.E. and D.E. degrees in electrical and communication engineering from Tohoku University, Sendai, Japan, in 2005 and 2010, respectively.

He has been a Research Associate at Tohoku University since 2010, prior to joining the Nagoya Institute of Technology, Nagoya, Japan, and Tokyo Metropolitan University, Tokyo, Japan, in 2011 and 2013, respectively. He is currently with the National Institute of Information and Communications Technology, Tokyo. His research interests include computational electromagnetics for biomedical communications and electromagnetic compatibility.

Dr. Chakarothai is a member of the Institute of Electronics, Information and Communication Engineers and the Institute of Electrical Engineers, Japan. He is also a member of the Bioelectromagnetic Society and the Applied Computational Electromagnetic Society. He was a recipient of the 2014 Young Scientist Award from the International Scientific Radio Union.

TATSUYA KASHIWA (M'88) was born in Hokkaido, Japan, in 1961. He received the B.S. and M.S. degrees in electrical engineering from Hokkaido University, Sapporo, Japan, in 1984 and 1986, respectively, and the Ph.D. degree.

In 1988, he joined the Department of Electrical Engineering as an Assistant Professor. In 1996, he joined the Department of Electrical and Electronic Engineering, Kitami Institute of Technology, as an Associate Professor, where he has been a Professor since 2008. He has co-authored the books *Handbook of Microwave Technology* (Academic Press), *Antennas and Associated Systems for Mobile Satellite Communications* (Research Signpost), and *Antennas for Small Mobile Terminals* (Artech House). His research interests include the analysis of electromagnetic and acoustic fields, electromagnetic compatibility, and optimization problems. He is a member of IEEJ and IEICE (fellow). He was a recipient of the IEEE AP-S Tokyo Chapter Young Engineer Award in 1992. He was the Chairman of Technical Committee on Electronics Simulation Technology, a member of the Technical Committee on Electromagnetic Theory and Microwaves of IEICE. He is a Task Force Chair of subcommittee of EMF Dosimetry Modeling under IEEE International Committee on Electromagnetic Safety.